Quantum State-to-State Rates for Multistate Processes from Coherences

Reshmi Dani[1] and Nancy Makri[1,2,3,*]

[1]*Department of Chemistry, University of Illinois, Urbana, Illinois 61801*
[2]*Department of Physics, University of Illinois, Urbana, Illinois 61801*
[3]*Illinois Quantum Information Science and Technology Center*

[*]*Corresponding Author. Email: nmakri@illinois.edu*

Abstract

For a multistate system coupled to a general environment through terms local in the system basis, we show that the time derivatives of populations are given in terms of imaginary components of coherences, i.e. off-diagonal elements of the reduced density matrix. When the process exhibits rate dynamics, we show that all state-to-state rates can be obtained from the early "plateau" values of these imaginary components. The evolution of the state populations is then obtained from the short-time simulation results and the solution of the kinetic equations with the computed rate matrix. These expressions generalize the reactive flux method and its non-equilibrium version to multi-state processes and show that even in the completely incoherent limit of rate kinetics, the time evolution of populations is governed by coherences. Further, we show that by virtue of detailed balance, the short-time values of the imaginary components of coherences fully determine the equilibrium populations.

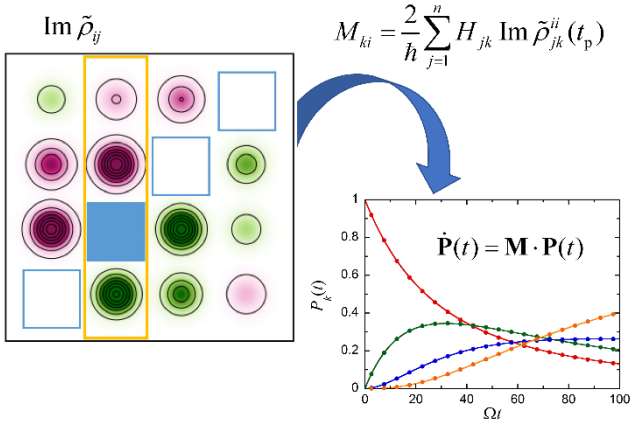

The determination of reaction rates from first principles has attracted much interest since the early days of quantum and statistical mechanics. In addition to difficulties involved in the electronic structure calculations required to obtain potential energy surfaces, the theoretical description of finite-temperature rate dynamics poses a challenging problem. Most efforts have focused either on barrier crossing[1] in the multidimensional potential energy surface that separates reactants from products, or on the rate of nonadiabatic transitions such as those relevant to electron transfer. An insightful picture of tunneling has emerged from semiclassical theory, which involves classical periodic orbits on the inverted barrier potential.[2] Analytical and numerical treatments have revealed a wealth of intriguing behaviors that characterize the dependence of the reaction rate for condensed phase processes on parameters, which include the Kramers turnover[3] along with the Grote-Hynes generalization[4-5] and its quantum mechanical extension,[6-7] the Marcus inverted regime,[8-9] as well as tunneling, curve crossing and quantum interference phenomena.[10-15]

Reaction rates are associated with exponential kinetics. In condensed-phase processes such behavior is observed when reactive processes are sufficiently slow in comparison to time scales associated with the reactants. If a particular state of the reactant configuration is prepared, the density relaxes very rapidly to a local equilibrium, before any measurable transformation to products has occurred. Under these conditions, the flux through a surface that divides reactants from products settles rapidly to a "plateau" value, from which a slow exponential decay is observed with the same time constant that characterizes the reactive process.[16] The reaction rate is then obtained from the plateau value of the reactive flux.[17-19] Classical[20] and quantum mechanical[21-22] equilibrium correlation function formulations have been developed for evaluating the flux that determines the reaction rate.

In this Letter we generalize these ideas to processes that involve transformations among multiple species. In this case rate kinetics can be described by simple kinetic equations that involve a matrix of state-to-state transition rates. The population evolution is then given by the exponential of this matrix, i.e. combinations of exponential functions characterized by rate constants. We show, most generally, that the time derivatives of populations are (at any time) simply related to the imaginary parts of off-diagonal reduced density matrix (RDM) elements (the "coherences"), and that the rates can be obtained from these imaginary components, which exhibit a plateau regime. Thus, even though the populations may obey classical-like kinetic equations, the underlying dynamics is always and entirely driven by the time evolution of coherences.

We consider the dynamics of discrete multistate Hamiltonians, which may represent a variety of processes, such as charge or energy transport, or condensed-phase reactive processes described by continuous potentials discretized along a reaction coordinate. In the case of a system described in terms of a continuous coordinate s (e.g. a double well potential), one may use the n lowest eigenstates of the system Hamiltonian to perform a unitary transformation to a discrete variable representation[23-24] (DVR), in which the coordinate operator is diagonal. The system operator in the DVR basis can be expressed in terms of its spectral expansion,

$$\hat{s} = \sum_{i=1}^{n} s_i \left|i\right\rangle\left\langle i\right| \tag{1}$$

where $|i\rangle$ are the n localized DVR states (or sites) and the DVR eigenvalues s_i serve as grid points. Thus, the Hamiltonian for discrete as well as (through this transformation) continuous systems is expressed in the form

$$\hat{H}_0 = \sum_{i=1}^{n}\sum_{j=1}^{n} H_{ij}\,|i\rangle\langle j| \tag{2}$$

with $H_{ij} = H_{ji}$. In addition to reactant-product processes, Eq. (2) can also be used to describe charge transport systems (where $|i\rangle$ represent electronic states in a diabatic representation), excitation energy transfer in molecular aggregates (where $|i\rangle$ are excited states of monomers), coupled spin systems, and many other situations. Typically, the system interacts with a large environment (the "bath") at a particular temperature through terms that are diagonal in the site basis. For example, local interactions occur in continuous potentials where the coupling is expressed in terms of the system coordinate *s*, in two- or multi-state charge transfer Hamiltonians in a diabatic representation, and in large molecular aggregates where the environment consists of vibrational modes of individual molecules. We do not impose any restrictions on the form of the bath Hamiltonian or the initial density matrix.

The RDM of the system (in the site representation) is given by

$$\tilde{\rho}_{km}(t) = \mathrm{Tr}_{\mathrm{b}}\left\langle k\left|e^{-i\hat{H}t/\hbar}\hat{\rho}(0)e^{i\hat{H}t/\hbar}\right|m\right\rangle \tag{3}$$

where $\hat{\rho}(0)$ is the initial density operator and the trace is with respect to the bath. The site populations P_k are given by the diagonal elements of the RDM, which may be written as

$$P_k(t) \equiv \tilde{\rho}_{kk}(t) = \mathrm{Tr}\left(e^{-i\hat{H}t/\hbar}\hat{\rho}(0)e^{i\hat{H}t/\hbar}|k\rangle\langle k|\right). \tag{4}$$

Taking the time derivative of Eq. (4), we obtain

$$\frac{d}{dt}P_k(t) = \frac{i}{\hbar}\mathrm{Tr}\left(e^{-i\hat{H}t/\hbar}\hat{\rho}(0)e^{i\hat{H}t/\hbar}\left[\hat{H},|k\rangle\langle k|\right]\right) \tag{5}$$

Since the system-bath coupling is diagonal in the site basis, only the system Hamiltonian contributes to the commutator. It is straightforward to see that Eq. (5) becomes

$$\frac{d}{dt}P_k(t) = \frac{i}{\hbar}\sum_{j=1}^{n}\left(H_{jk}\tilde{\rho}_{kj}(t) - H_{kj}\tilde{\rho}_{jk}(t)\right) \tag{6}$$

Using the Hermitian property of the Hamiltonian and the RDM, we arrive at the result

$$\frac{d}{dt}P_k(t) = \frac{2}{\hbar}\sum_{j=1}^{n} H_{jk}\,\mathrm{Im}\,\tilde{\rho}_{jk}(t)\,. \tag{7}$$

We emphasize that the populations and coherences are to be obtained from the same initial condition.

Eq. (7) is completely general and exact, regardless of the form of the bath Hamiltonian, as long as the system-bath coupling is diagonal in the system basis. It generalizes the expression obtained earlier[25] for a symmetric two-level system (TLS) and shows that in the absence of imaginary components in the coherences, populations remain stationary. This is always the situation at long times, when the process has reached equilibrium and the RDM elements are given by Boltzmann matrix elements, which are purely real-valued. In multistate systems this behavior is also observed at the start of the dynamics for a real-valued initial RDM. Conversely, if the system populations are evolving, some off-diagonal RDM elements *must* be complex-valued. Figure 1 illustrates Eq. (7).

Note that the imaginary parts of the coherences in the column containing a site population may at particular instants add to zero. These situations correspond to extrema (or inflection points) of the site population, at which its time derivative vanishes. Further, we note that at the start of the evolution and as long as the initial RDM is real-valued, Eq. (7) guarantees that the time derivatives of all site populations are equal to zero, implying that populations evolve at least quadratically in time as $t \to 0$. This is in line with the conclusions obtained in earlier work[26] on the evolution of purity and the RDM for a symmetric TLS coupled to a bath.

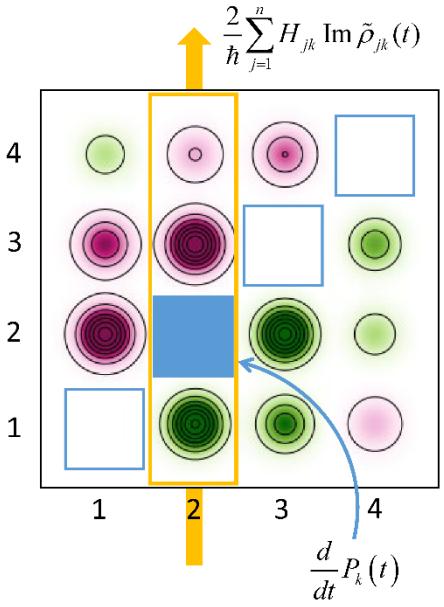

Fig. 1. Illustration of Eq. (7). Magenta and green areas show a visualization of positive and negative values of RDM imaginary parts in the case of a 4-state system coupled to a harmonic bath. The diagonal elements (blue squares) are purely real-valued. The time derivative of the population of the second site, indicated by a filled blue square, is proportional to the sum of Hamiltonian matrix elements multiplied by imaginary components inside the column outlined in yellow.

In condensed-phase processes rate kinetics are observed in strongly incoherent regimes if there is adequate separation of time scales. We now discuss how Eq. (7) can be used to determine rate constants in such situations. We begin with the standard reactant-product process described in terms of two states,

$$|1\rangle \underset{k_{-1}}{\overset{k_1}{\rightleftharpoons}} |2\rangle . \tag{8}$$

At sufficiently high temperatures and strong system-bath coupling, the site populations rapidly settle into forms that satisfy kinetic equations. The two populations can then be described in terms of a forward and a reverse rate constant through the simple differential equations

$$\begin{aligned} \dot{P}_1(t) &= -k_1 P_1(t) + k_{-1} P_2(t) \\ \dot{P}_2(t) &= k_1 P_1(t) - k_{-1} P_2(t) \end{aligned} \tag{9}$$

whose solution gives exponential population evolution,

$$\begin{aligned} P_1(t) - P_1(\infty) &= \left[P_1(0) - P_1(\infty)\right] e^{-(k_1 + k_{-1})t} \\ P_2(t) - P_2(\infty) &= \left[P_2(0) - P_2(\infty)\right] e^{-(k_1 + k_{-1})t} \end{aligned} \tag{10}$$

In this case, knowledge of the forward and reverse rates is sufficient to fully characterize the dynamics, including the equilibrium constant $K = P_2(\infty) / P_1(\infty) = k_1 / k_{-1}$ (i.e. the populations of the two species when equilibrium has been reached).

Exponential population dynamics requires a separation of time scales, implying that the time required for the system populations to reach equilibrium is much longer than the time of local equilibration with the environment, allowing the populations to enter a regime of exponential decay early on, i.e. long before appreciable deviations from their initial values have occurred, and Eq. (10) is valid excluding a very short interval of nonexponential transients.[16] This realization has led to the development of classical and quantum mechanical flux correlation function formulations,[20-22] which deduce the rate from the behavior of the flux in the "plateau" regime. The standard formulation is based on the equilibrium flux correlation function, but recent work has shown[27] that the flux obtained with non-equilibrium initial conditions contains precisely the same information and may be used to obtain the rate without the need for numerical evaluation of the full equilibrium density. Specifically, if $P_1(0) = 1$, Eq. (10) gives

$$\dot{P}_1(t) = -\left(k_1 + k_{-1}\right)\left[1 - P_1(\infty)\right] e^{-(k_1 + k_{-1})t} = -k_1 e^{-(k_1 + k_{-1})t}, \quad t > t_{\mathrm{p}} . \tag{11}$$

$\dot{P}_1$ is the non-equilibrium flux, which (for a real-valued initial RDM) vanishes at the start of the evolution. Using Eq. (7), this function may be obtained from the imaginary part of the off-diagonal element of the RDM. Since $\exp(-k_1 t_{\mathrm{p}} - k_{-1} t_{\mathrm{p}}) \simeq 1$, the non-equilibrium flux quickly grows from zero to the value given by the right-hand side of Eq. (10) at the onset t_{p} of the plateau regime, after which it decays exponentially over a time that is very long compared to t_{p}. Assuming, as usual, that the exponential factor is very close to unity at this time, we recover the result[25]

$$k_1 = \frac{2}{\hbar} H_{12} \operatorname{Im} \tilde{\rho}_{12}(t_{\mathrm{p}}) . \tag{12}$$

We now proceed to generalize these ideas to processes that involve multiple states, in regimes where the populations obey rate kinetics. Consider a general system of *n* states which are coupled through the Hamiltonian given by Eq. (2) and whose populations satisfy kinetic equations,

$$\frac{d}{dt}\mathbf{P}(t) = \mathbf{M}\cdot\mathbf{P}(t) \tag{13}$$

where $\mathbf{P}(t)$ is the vector that contains the populations P_k of the states at time *t* and **M** is a matrix of transition rates. Using Eq. (7), we obtain

$$\dot{P}_k(t) = \sum_{j=1}^{n} M_{kj} P_j(t) = \frac{2}{\hbar}\sum_{j=1}^{n} H_{jk}\,\mathrm{Im}\,\tilde{\rho}_{jk}(t)\ . \tag{14}$$

This equation holds for any initial condition of the RDM. We now evaluate Eq. (14) with *all* initial conditions, $\hat{\rho}(0) = |i\rangle\langle i|$, at the plateau time. We indicate the initial condition in the RDM elements through a superscript, $\tilde{\rho}^{ii}_{jk}$. Using again $P_i \simeq 1, P_{j\neq i} \simeq 0$ at the early plateau time, we obtain

$$\frac{d}{dt}\tilde{\rho}^{ii}_{kk}(t_{\mathrm{p}}) = M_{ki} \tag{15}$$

which leads to the result

$$M_{ki} = \frac{2}{\hbar}\sum_{j=1}^{n} H_{jk}\,\mathrm{Im}\,\tilde{\rho}^{ii}_{jk}(t_{\mathrm{p}})\,. \tag{16}$$

Eq. (16) gives the state-to-state rates in terms of the (imaginary parts of) coherences at the plateau time.

We note that while the matrix **M** has n^2 elements, there are only $n(n-1)$ forward and reverse rate constants. This implies that there is redundancy (i.e. linear dependence) in this matrix, i.e. $\det(\mathbf{M}) = 0$. Differentiating the sum of populations, one can express a diagonal element M_{kk} in terms of all other elements M_{jk}. This allows the kinetic equations to be written in a form that does not involve diagonal elements,

$$\dot{P}_k(t) = \sum_{j\neq k}^{n} M_{kj} P_j(t) - \left(\sum_{j\neq k}^{n} M_{jk}\right) P_k(t)\,, \tag{17}$$

implying that only $n^2 - n$ elements of the matrix are required to fully characterize the kinetics. With $j \neq k$ the elements of **M** are the forward and reverse rate constants between sites. If the basis states are used only as a discretization of a continuous system coordinate the individual rates may not have a direct physical meaning, but may be summed to give reactant-to-product rates (for example, to describe the rate dynamics between the left and right regions of a double well potential).

The system of differential equations involves the exponential of this matrix, thus the individual populations involve multiple exponential components. The relevant time scales are given by (reciprocals

of) the eigenvalues of the rate matrix **M**. Since the determinant of the rate matrix vanishes, one eigenvalue is always equal to zero, indicating that the map of Eq. (13) has a fixed point. The corresponding eigenvector determines the composition of the equilibrium RDM.

Further, we note that in cases of imperfect separation of timescales, the populations may have deviated significantly from their initial values during the short time of transient evolution that precedes the plateau regime. The kinetic equations are valid for $t > t_{\mathrm{p}}$ and should be integrated with adjusted initial conditions given by the actual value of $P_k(t_{\mathrm{p}})$, while the population values obtained from the full propagation of the RDM should be used for $t < t_{\mathrm{p}}$.

Last, the detailed balance property states that

$$M_{ki} P_i(\infty) = M_{ik} P_k(\infty) \tag{18}$$

which implies that *the imaginary parts of the coherences at the plateau time fully specify the equilibrium populations* through the relation

$$\sum_{j=1}^{n} H_{jk} \operatorname{Im} \tilde{\rho}_{jk}^{ii}(t_{\mathrm{p}}) P_i(\infty) = \sum_{j=1}^{n} H_{ji} \operatorname{Im} \tilde{\rho}_{ji}^{kk}(t_{\mathrm{p}}) P_k(\infty) . \tag{19}$$

This property is subtle and rather remarkable.

As an example, consider a three-state system where all states are coupled in the Hamiltonian, describing a physical situation where the transformation from $|1\rangle$ to $|3\rangle$ can occur through two pathways, i.e. through direct population transfer as well as through an intermediate state $|2\rangle$. We label the rate constants symmetrically,

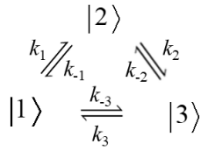

(20)

The kinetic equations for the evolution of the populations can be written in terms of six rate constants,

$$\begin{aligned}
\dot{P}_1(t) &= -k_1 P_1(t) + k_{-1} P_2(t) + k_3 P_3(t) - k_{-3} P_1(t) \\
\dot{P}_2(t) &= k_1 P_1(t) - k_{-1} P_2(t) - k_2 P_2(t) + k_{-2} P_3(t) \\
\dot{P}_3(t) &= k_2 P_2(t) - k_{-2} P_3(t) - k_3 P_3(t) + k_{-3} P_1(t)
\end{aligned} \tag{21}$$

The rate equations can be cast in the matrix form of Eq. (13) with the identifications $M_{12} = k_{-1}$, $M_{13} = k_3$, $M_{21} = k_1$, $M_{23} = k_{-2}$, $M_{31} = k_{-3}$, $M_{32} = k_2$. Evaluating $\dot{P}_k$ for all initial conditions $\hat{\rho}(0) = |i\rangle\langle i|$, $i \neq k$, we obtain

$$k_1 = \frac{2}{\hbar} H_{12}\,\mathrm{Im}\,\tilde{\rho}_{12}^{11}(t_\mathrm{p}) + \frac{2}{\hbar} H_{32}\,\mathrm{Im}\,\tilde{\rho}_{32}^{11}(t_\mathrm{p}), \quad k_{-1} = \frac{2}{\hbar} H_{21}\,\mathrm{Im}\,\tilde{\rho}_{21}^{22}(t_\mathrm{p}) + \frac{2}{\hbar} H_{31}\,\mathrm{Im}\,\tilde{\rho}_{31}^{22}(t_\mathrm{p})$$
$$k_2 = \frac{2}{\hbar} H_{23}\,\mathrm{Im}\,\tilde{\rho}_{23}^{22}(t_\mathrm{p}) + \frac{2}{\hbar} H_{13}\,\mathrm{Im}\,\tilde{\rho}_{13}^{22}(t_\mathrm{p}), \quad k_{-2} = \frac{2}{\hbar} H_{12}\,\mathrm{Im}\,\tilde{\rho}_{12}^{33}(t_\mathrm{p}) + \frac{2}{\hbar} H_{32}\,\mathrm{Im}\,\tilde{\rho}_{32}^{33}(t_\mathrm{p}) \tag{22}$$
$$k_3 = \frac{2}{\hbar} H_{21}\,\mathrm{Im}\,\tilde{\rho}_{21}^{33}(t_\mathrm{p}) + \frac{2}{\hbar} H_{31}\,\mathrm{Im}\,\tilde{\rho}_{31}^{33}(t_\mathrm{p}), \quad k_{-3} = \frac{2}{\hbar} H_{23}\,\mathrm{Im}\,\tilde{\rho}_{23}^{11}(t_\mathrm{p}) + \frac{2}{\hbar} H_{13}\,\mathrm{Im}\,\tilde{\rho}_{13}^{11}(t_\mathrm{p})$$

The expressions in Eq. (22) agree with the general form given by Eq. (16). The diagonal components in Eq. (21) are $M_{11} = -k_1 - k_{-3}$, $M_{22} = -k_{-1} - k_2$ and $M_{33} = -k_{-2} - k_3$, i.e. are given in terms of sums of off-diagonal elements of the rate matrix, thus are not independent, in agreement with the remark made earlier.

If all coupling elements have the same value, the three-site system is completely symmetric and all rate constants are identical. In this case the eigenvector corresponding to the vanishing eigenvalue of **M**, which describes the equilibrium populations, has equal components on the three sites. Symmetry breaking (through nondegenerate site energies or unequal coupling matrix elements) leads to unequal site populations. A non-cyclic tight binding Hamiltonian (for example Eq. (24) below) with identical nearest neighbor couplings has different forward and reverse rates, which become equal only at infinite temperature, thus in general the equilibrium populations of each site depend on the location of the site.

To illustrate these ideas, we present numerical results on several models of discrete systems coupled to separate harmonic baths (which might correspond to intramolecular normal mode coordinates of molecular aggregates[28]) characterized by the spectral density function[29]

$$J(\omega) = \tfrac{1}{2}\pi\xi\omega e^{-\omega/\omega_\mathrm{c}}, \tag{23}$$

which peaks at the frequency ω_c and where ξ is the dimensionless Kondo parameter that quantifies the system-bath coupling strength. In all cases the bath is initially equilibrated with respect to a common ground state, as in the case of energy transfer following a Franck-Condon initial excitation.

We describe the models in terms of a characteristic coupling value $\hbar\Omega$ between system sites. To generate conditions for a reasonable separation of time scales we present results for $\omega_\mathrm{c} = 100\,\Omega$. We use two values of the Kondo parameter, $\xi = 0.1$ and 0.5, which correspond to reorganization energies equal to $20\hbar\Omega$ and $100\hbar\Omega$, respectively. To put these values in the context of chemical processes, it is useful to consider the value $2\hbar\Omega \simeq 10\ \mathrm{cm}^{-1}$ as a tunneling splitting typical of many proton transfer or isomerization processes. With this value of Ω, the characteristic bath frequency corresponds to 500 cm^{-1} and the reorganization energy is $100\,\mathrm{cm}^{-1}$ with $\xi = 0.1$ and $500\,\mathrm{cm}^{-1}$ if $\xi = 0.5$. In the calculations shown in Figures 2-5 we obtain an adequate plateau at or above the intermediate temperature $\hbar\omega_\mathrm{c}\beta = 2$, which is slightly higher than room temperature. We note that the temperature is very high with respect to the characteristic frequency of the system, i.e. $\hbar\Omega\beta = 0.02$. As a result, all site populations attain equal values of $1/n$ at equilibrium.

We also consider a slower bath with $\omega_\mathrm{c} = 10\,\Omega$. This relatively low-frequency bath does not produce a good separation of time scales and the flux does not exhibit a flat plateau. For the same system energy scale $2\hbar\Omega \simeq 10\ \mathrm{cm}^{-1}$, the characteristic frequency of the bath is now only 50 cm^{-1}, typical of solvent modes. Nevertheless, we show that at the same temperature (for which now $\hbar\omega_\mathrm{c}\beta = 0.2$), the population evolution is still quantitatively described by kinetic equations and the rates obtained from the sloped flux function are highly accurate. On the other hand, if the system energy scale is characteristic of

Frenkel exciton[30] couplings, $\hbar\Omega \simeq 50$ cm^{-1}, a bath frequency $\omega_c = 10\,\Omega$ corresponds to 500 cm^{-1}. Realistic temperatures in this case correspond to $\hbar\omega_c\beta = 2$ or higher. As the temperature is decreased, time scales become truly mixed, eventually causing a breakdown of the kinetic equations.

The real time dynamics of the system was performed using the small matrix decomposition of the path integral[31-33] (SMatPI). This is an exact, analytically derived decomposition of the quasi-adiabatic propagator path integral[34] (QuAPI) which allows iterative propagation with small, $n^2 \times n^2$ matrices, thereby obviating the tensor storage of the iterative QuAPI algorithm.[35-36] The real-time path integral[37-38] is an exact, fully quantum mechanical formulation of time-dependent quantum mechanics that allows an analytical treatment of harmonic bath degrees of freedom without approximation.[39] The SMatPI algorithm employs two convergence parameters, the memory length L and the entanglement length $r_{\max}$, which in many situations is shorter than the memory induced by the bath.[33,40] The coupled kinetic equations were solved using the numerical differential equation solver of Mathematica.[41]

Figures 2-5 show the time evolution of the site populations that develop from the initial condition $\tilde{\rho}(0) = |1\rangle\langle 1|$, as well as their time derivatives, as obtained from the SMatPI calculations and also from solving the kinetic equations with the rates obtained from the imaginary parts of the coherences, for several multistate model systems. In all cases it is seen that the time derivatives obtained from Eq. (7) agree exactly with those obtained through numerical differentiation of the SMatPI population results at all times. Further, the solution of the kinetic equations with rates obtained from the imaginary parts of the coherences are in excellent agreement with the SMatPI results.

In the first model (Figure 2) we use a three-state system with identical site energies and nearest-neighbor couplings, described by the Hamiltonian

$$\hat{H}_0 = -\hbar\Omega\left(|1\rangle\langle 2| + |2\rangle\langle 1| + |2\rangle\langle 3| + |3\rangle\langle 2|\right), \tag{24}$$

which describes a sequential process. The bath is at the intermediate temperature $\hbar\omega_c\beta = 2$. We consider two values of the bath frequency, $\omega_c = 100\,\Omega$ and $10\,\Omega$, along with two values of the Kondo parameter. In all cases the populations of the first two sites start changing immediately, while the third site follows later, with a zero derivative at the initial time. On the time scale that corresponds to completion of the process, the populations, as well as the imaginary parts of the coherences (as time derivatives of populations), exhibit (multi-)exponential evolution. However, the imaginary components of the coherences are seen to rise very steeply before settling into their slow evolution and eventual decay. Upon magnification, a near-plateau, i.e. a linear region with a very small slope which is established at the early time $\Omega t_p \simeq 0.1 - 0.2$. This linear shape is the short-time expansion of the exponential population derivatives. We note that an even larger value of ω_c would result in a more pronounced separation of timescales and a truly flat (on the time scale of these graphs) plateau region in the population derivatives.

The dynamics is faster with smaller values of the reorganization energy ($\xi = 0.1$ and $\omega_c = 10\,\Omega$), causing a more conspicuous slope of the time derivatives. Even in the absence of a perfect plateau, the population dynamics reproduced by the rates obtained from the imaginary parts of the coherences match the path integral results perfectly. With the smaller value of system-bath coupling ($\xi = 0.1$), the evolution of population derivatives is nearly monotonic up to the plateau value. In contrast, the population derivatives undergo strongly nonmonotonic evolution prior to reaching the plateau when the reorganization energy is large ($\xi = 0.5$). The slower population dynamics observed in this case leads to a flatter plateau regime.

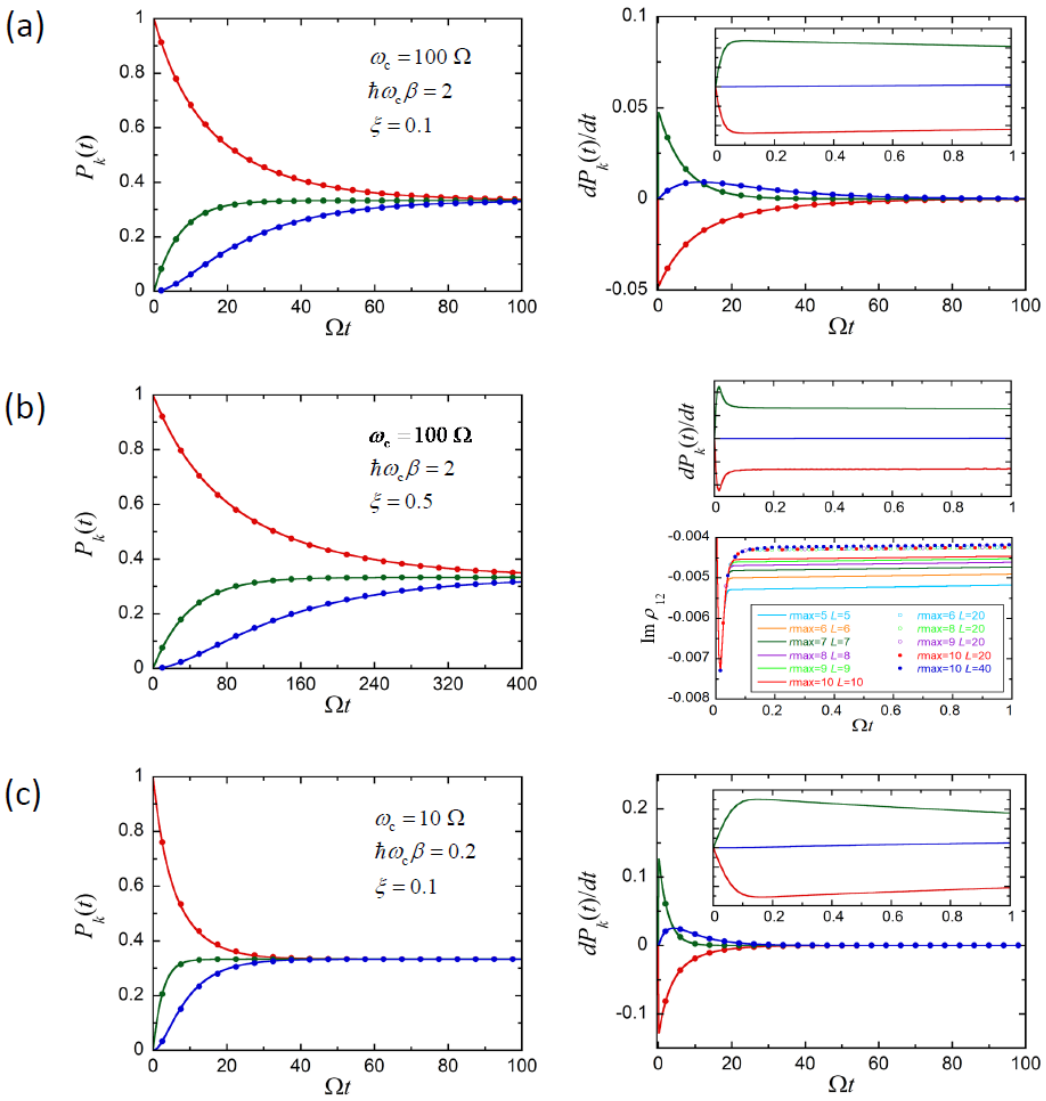

Fig. 2. Site populations and their derivatives for the three-state model with the Hamiltonian given by Eq. (24). Solid lines show SMatPI results for the site populations and their numerical derivatives computed by finite difference. In the right panels, markers show the population derivatives obtained from the imaginary parts of the coherences, while in the left panels, markers show populations obtained from the solution of the kinetic equations with rates computed from the coherences at the plateau time. The insets show enlargements of the early dynamics. In (b) the right panel shows the convergence of the imaginary component of a coherence as a function of the SMatPI entanglement parameter $r_{\max}$ and the memory length L. Red, green and blue correspond to sites 1, 2 and 3, respectively. (a) $\omega_c = 100\Omega$, $\xi = 0.1$, $\hbar\omega_c\beta = 2$. (b) $\omega_c = 100\Omega$, $\xi = 0.5$, $\hbar\omega_c\beta = 2$. (c) $\omega_c = 10\Omega$, $\xi = 0.1$, $\hbar\omega_c\beta = 0.2$.

In all cases shown in Fig. 2, the RDM needs to be propagated for a relatively short time. This time should be longer than t_p ($\Omega t \sim 1$ in the present example) to verify the existence of a rate plateau. With the value $\xi = 0.5$, converged SMatPI results were obtained with a time step $\Omega\Delta t = 0.005$, entanglement length $r_{\max} = 10$ and memory length $L = 40$. With this time step, propagation to the time $\Omega t = 1$ required to establish the plateau involves 200 iteration steps, while propagation to the time

$\Omega\Delta t = 400$ shown in the figure involves 80000 iterations. The SMatPI iteration algorithm is stable and extremely fast, so this propagation length does not present any difficulties. However, iteration to such long times would be challenging if the process involved a complex, anharmonic environment.

Next, we show (in Fig. 3) results for a different three-state process, where state 1 is transformed to 3 through the direct pathway and also through an intermediate (state 2) according to the Hamiltonian

$$\hat{H}_0 = -\tfrac{1}{2}\hbar\Omega\left(|1\rangle\langle 2| + |2\rangle\langle 1|\right) - \hbar\Omega\left(|2\rangle\langle 3| + |3\rangle\langle 2|\right) - \tfrac{3}{2}\hbar\Omega\left(|1\rangle\langle 3| + |3\rangle\langle 1|\right). \tag{25}$$

In this case, population is transferred to states 2 and 3 simultaneously but with different rates, as expected based on the different coupling strengths to state 1. In Fig. 3a the bath parameters and temperature are identical to those of Fig. 2a, yet the dynamics is considerably faster because of the existence of two pathways and the larger value of one of the couplings. As a result, the separation of time scales is weaker in this case, giving rise to a somewhat larger slope of the flux in the plateau regime. Nevertheless, the computed rates again give rise to highly accurate populations, which are practically identical to those from the SMatPI results.

In the case of a two-state system with weak coupling to a harmonic bath, a decrease of temperature leads to larger rate.[10,14] This trend is observed in the three-site dynamics as well. As the temperature is lowered, early-time transients survive much longer and merging time scales lead to deviations from uniform exponential behavior, affecting the accuracy of kinetic equation models. Fig. 3b shows results at the temperature $\hbar\omega_c\beta = 5$, which is lower than the previous temperatures, although still relatively high with respect to the system energy scales ($\hbar\Omega\beta = 0.5$). Even though the time for completion of this process is comparable to that in Fig. 2c, the flux rises much slower in the present case and settles to a less defined plateau much later ($\Omega t_p \simeq 0.6$). The populations obtained from the kinetic equations with rates extracted from the coherences deviate from the correct dynamics. However, initializing the kinetic equations with the population values from the path integral results at t_p leads to improved results which are almost quantitative. Further decrease of the temperature leads to oscillatory dynamics through inadequate damping of quantum coherence, which invalidate the kinetic equations.

We now move on to a four-state downhill process, where the Hamiltonian has nearest-neighbor couplings but the site energies decrease gradually according to the Hamiltonian

$$\hat{H}_0 = -\hbar\Omega\sum_{i=1}^{3}\left(|i\rangle\langle i+1| + |i+1\rangle\langle i|\right) - 50\hbar\Omega|2\rangle\langle 2| - 100\hbar\Omega|3\rangle\langle 3| - 150\hbar\Omega|4\rangle\langle 4|. \tag{26}$$

Fig. 4 shows the results for this process. Here the site populations rise sequentially, and those of sites 3 and 4 (which are not directly coupled to 1) have a zero slope at early times. State 2 shows a pronounced peak in the population, while that of state 4 rises monotonically. In this case the equilibrium populations decrease monotonically from 1 to 4 because the temperature is moderate to low with respect to differences in site energies, $\hbar(150\Omega)\beta = 3$.

Last, we present results for a 10-site system with nearest-neighbor couplings described by

$$\hat{H}_0 = -\hbar\Omega\sum_{i=1}^{9}\left(|i\rangle\langle i+1| + |i+1\rangle\langle i|\right) \tag{27}$$

with the parameters of Fig. 2a ($\hbar\omega_c\beta = 2$, $\omega_c = 100\ \Omega$ and $\xi = 0.1$). Figure 5 shows the site populations, which rise in sequence. Again, the rates computed from the imaginary parts of the coherences lead to excellent agreement between kinetic equations and path integral results.

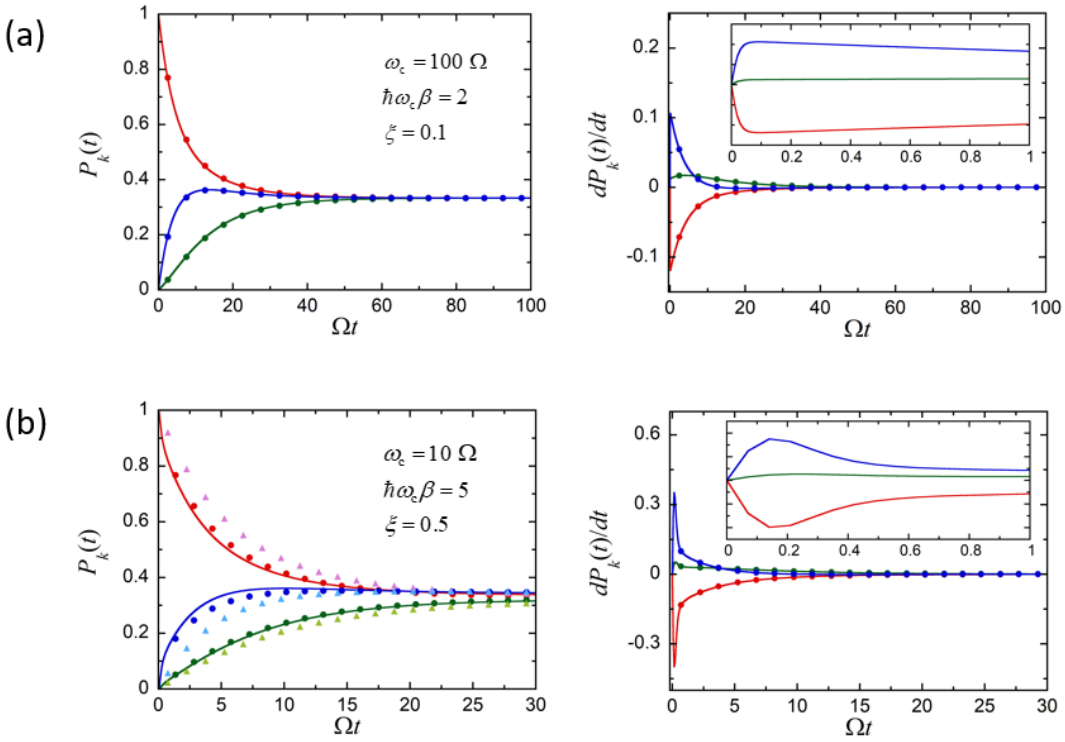

Fig. 3. Site populations and their derivatives for the three-state model with the Hamiltonian given by Eq. (25). Solid lines show SMatPI results for the site populations and their numerical derivatives computed by finite difference. In the right panels, markers show the population derivatives obtained from the imaginary parts of the coherences, while in the left panels, they show populations obtained from the solution of the kinetic equations with rates computed from the coherences at the plateau time. In (b), triangles show results obtained by integrating the kinetic equation from $t = 0$, while circles show solutions obtained after the t_p, while early time populations are obtained from SMatPI results. The insets show enlargements of the early dynamics. Red, green and blue correspond to sites 1, 2 and 3, respectively. (a) $\omega_c = 100\Omega$, $\xi = 0.1$, $\hbar\omega_c\beta = 2$. (b) $\omega_c = 10\Omega$, $\xi = 0.1$, $\hbar\omega_c\beta = 5$.

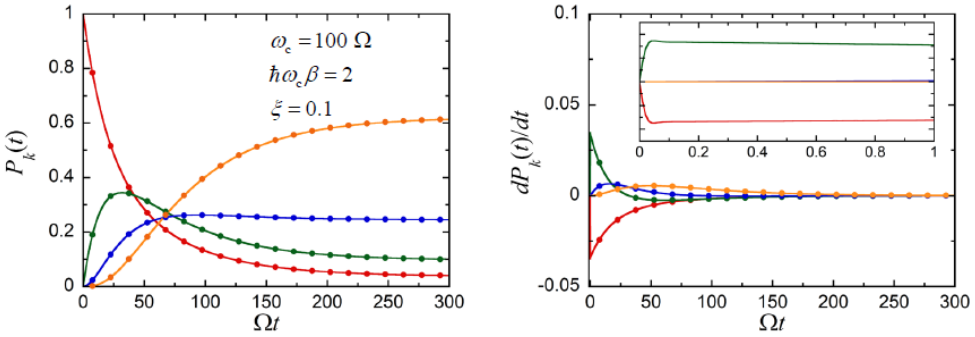

Fig. 4. Same as Fig. 3, but for the four-state system given in Eq. (26). The parameters are $\omega_c = 100\Omega$, $\xi = 0.1$, $\hbar\omega_c\beta = 2$. Red, green, blue and orange correspond to sites 1, 2, 3 and 4, respectively.

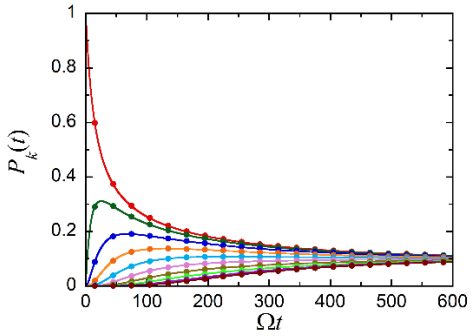

Fig. 5. Site populations for the ten-state model with the Hamiltonian given by Eq. (27) with $\omega_c = 100\Omega$, $\xi = 0.1$, $\hbar\omega_c\beta = 2$. Solid lines show SMatPI results for the site populations, while markers show populations obtained from the solution of the kinetic equations with rates computed from the coherences at the plateau time. The populations of sites 2-10 rise in sequence.

A few remarks are in order before summarizing. First, the simple master equation describes Markovian dynamics. However, this does not imply that the rate constants can be calculated from a Markovian algorithm. This is so because the early time evolution, prior to the onset of the plateau regime, is non-Markovian. Thus, the determination of the rate matrix generally requires the use of powerful quantum dynamical methods.

Second, the validity of a set of simple kinetic equations with available rate parameters is important conceptually and, in the case of processes in complex, anharmonic environments, quite useful from a practical perspective. For very slow (>ns time scale) processes, knowledge of the rate matrix usually is sufficient. Obtaining the full time evolution of site populations can be useful in multistate processes, in particular when competing pathways are available. This can be done very easily through numerical integration of the kinetic equations. We note that in the case of a system coupled to a harmonic bath, iterative propagation of the RDM is performed extremely rapidly with the SMatPI algorithm, which involves repeated multiplication of $n^2 \times n^2$ matrices and which remains stable for tens of thousands of propagation steps. However, the kinetic equation approach should be more efficient for multistate systems ($n > 10$) and/or very slow processes. Most importantly, the cost of long-time propagation generally is much higher when the system is coupled to a complex anharmonic environment. In this case, calculating the relatively short-time dynamics of the RDM that encodes the rate information via a reliable method and obtaining long-time populations by solving the coupled kinetic equations would be the most efficient approach, as long as the kinetic equation description is applicable.

In summary, when the interaction between a system and its environment is local in the system basis, imaginary components of coherences are directly related to time derivatives of populations. Each such time derivative can be thought of as a state-to-state flux, which (under conditions associated with rate dynamics) settles early on to a slow exponential decay with the usual plateau appearance familiar from reaction rate theory. The imaginary component of the multistate RDM (with all possible initial conditions) at the relatively short plateau time determines the state-to-state rate matrix, which may be used to obtain the population dynamics by solving a system of simple kinetic equations. We found the

procedure to be robust and accurate even when the plateau is visibly sloped and the onset of the plateau regime occurs later, as long as the kinetic equations are used only for the remainder of the time evolution.

Even when systems exhibit rate kinetics associated with classical hopping models, our analysis reveals that quantum coherences are present during the entire course of time evolution. Coherences are associated with quantum superpositions, which survive the massive damping that gives rise to exponential evolution. More severe damping of superpositions leads to slower dynamics. When thermal fluctuations and noisy environments drastically quench coherent superpositions of states, quantum transitions become very slow, leading to small rates. Thus, phenomenological kinetic equations emerge when noise dampens quantum superpositions extensively, creating slow processes and a separation of time scales that lead to exponential evolution, and not because of the absence of quantum effects.

Since state-to-state rates determine equilibrium populations by virtue of the detailed balance property, we concluded that (for processes that exhibit rate kinetics) the early time evolution of coherences also encodes all information necessary for obtaining the populations at equilibrium. This striking observation applies to general multistate systems in contact with complex environments.

Acknowledgments

This material is based upon work supported by the National Science Foundation under Award CHE-1955302.

References

1. Fleming, G. R.; Hänggi, P., *Activated barrier crossing*. World Scientific: Singapore, 1993.
2. Miller, W. H., Semiclassical Limit of Quantum Mechanical Transition State Theory for Non-Separable Systems. *J. Chem. Phys.* **1975,** *62*, 1899-1906.
3. Kramers, H. A., Brownian motion an a field of force and the diffusion model of chemical reactions. *Physica (Utrecht)* **1940,** *7*, 284-304.
4. Grote, R. F.; Hynes, J. T., *J. Chem. Phys.* **1980,** *73*, 2715.
5. Pollak, E., Theory of activated rate processes: A new derivation of Kramers' expression. *J. Chem. Phys.* **1986,** *85*, 865.
6. Wolynes, P. G., Quantum theory of activated events in condensed phases. *Phys. Rev. Lett.* **1981,** *47*, 968.
7. Pollak, E.; Grabert, H.; Hänggi, P., Theory of activated rate processes for arbitrary frequency dependent friction: Solution of the turnover problem. *The Journal of Chemical Physics* **1989,** *91* (7), 4073-4087.
8. Marcus, R. A., Electrostatic free energy and other properties of states having nonequilibrium polarization. I. *J. Chem. Phys.* **1956,** *24*, 979-989.
9. Marcus, R. A.; Sutin, N., Electron transfers in chemistry and biology. *Biochim. Biophys. Acta* **1985,** *811*, 265-322.
10. Leggett, A. J.; Chakravarty, S.; Dorsey, A. T.; Fisher, M. P. A.; Garg, A.; Zwerger, M., Dynamics of the dissipative two-state system. *Rev. Mod. Phys.* **1987,** *59*, 1-85.
11. Frauenfelder, H.; Wolynes, P. G., Rate theories and puzzles of heme protein kinetics. *Science* **1985,** *228*, 337.
12. Onuchic, J. N.; Wolynes, P. G., Classical and quantum pictures of reaction dynamics in condensed matter: Resonances, dephasing, and all that. *J. Phys. Chem.* **1988,** *92*, 6495-6503.
13. Hänggi, P.; Talkner, P.; Borcovec, M., Reaction rate theory: Fifty years after Kramers. *Rev. Mod. Phys.* **1990,** *62*, 251-341.
14. Topaler, M.; Makri, N., Quantum rates for a double well coupled to a dissipative bath: accurate path integral results and comparisons with approximate theories. *J. Chem. Phys.* **1994,** *101*, 7500-7519.
15. Topaler, M.; Makri, N., Path integral calculation of quantum nonadiabatic rates in model condensed phase reactions. *J. Phys. Chem.* **1996,** *100*, 4430-36.
16. Chandler, D., *Introduction to Modern Statistical Mechanics*. Oxford University Press: New York, 1987.
17. Keck, J. C., Variational Theory of Chemical Reaction Rates Applied to Three-Body Recombinations *J. Chem. Phys.* **1960,** *32*, 1035.
18. Kapral, R., Internal Relaxation in Chemically Reacting Fluids. *J. Chem. Phys.* **1972,** *56*, 1842.
19. Chandler, D., Statistical mechanics of isomerization dynamics in liquids and the transition state approximation. *J. Chem. Phys.* **1978,** *68*, 2959-2970.
20. Berne, B. J., Methods in Rate Theory. In *Activated Barrier Crossing: Application in Physics, Chemistry and Biology*, Fleming, G. R.; Hänggi, P., Eds. World Scientific Publishing Co. Pt. Ltd.: Singapore, 1993; pp 82-119.
21. Yamamoto, T., Quantum Statistical Mechanical Theory of the Rate of Exchange Chemical Reactions in the Gas Phase. *J. Chem. Phys.* **1960,** *33*, 281-289.
22. Miller, W. H.; Schwartz, S. D.; Tromp, J. W., Quantum mechanical rate constants for bimolecular reactions. *J. Chem. Phys.* **1983,** *79*, 4889-4898.
23. Light, J. C.; Hamilton, I. P.; Lill, J. V., Generalized discrete variable approximation in quantum mechanics. *J. Chem. Phys.* **1985,** *82*, 1400-1409.
24. Echave, J.; Clary, D. C., Potential optimized discrete variable representation. *J. Chem. Phys.* **1992,** *190*, 225-230.
25. Chatterjee, S.; Makri, N., Recovery of purity in dissipative tunneling dynamics. *J. Phys. Chem. Lett.* **2020,** *11*, 8592-8596.

26. Chatterjee, S.; Makri, N., Density matrix and purity evolution in dissipative two-level systems: I. Theory and path integral results for tunneling dynamics. *Phys. Chem. Chem. Phys.* **2021,** *23*, 5113-5124.
27. Bose, A.; Makri, N., Non-equilibrium reactive flux: A unified framework for slow and fast reaction kinetics. *J. Chem. Phys.* **2017,** *147*, 152723.
28. Kundu, S.; Makri, N., Intramolecular Vibrations in Excitation Energy Transfer: Insights from Real-Time Path Integral Calculations. *Annual Review of Physical Chemistry* **2022,** *73* (1), 349-375.
29. Caldeira, A. O.; Leggett, A. J., Path integral approach to quantum Brownian motion. *Physica A* **1983,** *121*, 587-616.
30. Frenkel, J., On the transfomation of light into heat in solids. *Phys. Rev.* **1931,** *37*, 17.
31. Makri, N., Small matrix disentanglement of the path integral: overcoming the exponential tensor scaling with memory length. *J. Chem. Phys.* **2020,** *152*, 041104.
32. Makri, N., Small matrix path integral for system-bath dynamics. *Journal of Chemical Theory and Computation* **2020,** *16*, 4038–4049.
33. Makri, N., Small matrix path integral with extended memory. *J. Chem. Theory and Comput.* **2021,** *17*, 1-6.
34. Makri, N., Numerical path integral techniques for long-time quantum dynamics of dissipative systems. *J. Math. Phys.* **1995,** *36*, 2430-2456.
35. Makri, N.; Makarov, D. E., Tensor multiplication for iterative quantum time evolution of reduced density matrices. I. Theory. *J. Chem. Phys.* **1995,** *102*, 4600-4610.
36. Makri, N.; Makarov, D. E., Tensor multiplication for iterative quantum time evolution of reduced density matrices. II. Numerical methodology. *J. Chem. Phys.* **1995,** *102*, 4611-4618.
37. Feynman, R. P., Space-time approach to non-relativistic quantum mechanics. *Rev. Mod. Phys.* **1948,** *20*, 367-387.
38. Feynman, R. P.; Hibbs, A. R., *Quantum Mechanics and Path Integrals*. McGraw-Hill: New York, 1965.
39. Feynman, R. P.; Vernon, F. L., The theory of a general quantum system interacting with a linear dissipative system. *Ann. Phys.* **1963,** *24*, 118-173.
40. Kundu, S.; Dani, R.; Makri, N., B800-to-B850 relaxation of excitation energy in bacterial light harvesting: All-state, all-mode path integral simulations. *J. Chem. Phys.* **2022,** *157*, 115101.
41. Wolfram Research, I. *Mathematica*, Wolfram Research, Inc.: Champaign, Illinois, 2016.